sustainability

MDPI

Article

Aeolian Sand Test with True Triaxial Stress Path Achieved by Pseudo-Triaxial Apparatus

Zhigang Ma [1,2] and Xuefeng Li [1,2,*]

[1] School of Physics and Electronic-Electrical Engineering, Ningxia University, Yinchuan 750021, China; mazhigangl@163.com
[2] Solid Mechanics Institute, Ningxia University, Yinchuan 750021, China
* Correspondence: lixuefeng1928@163.com

Abstract: Aeolian sand is a special roadbed filler, but its three-dimensional mechanical properties are rarely studied. To obtain the characteristic of its deformation, strength on the deviatoric plane, and failure in three dimensions, a series of triaxial drained tests on aeolian sand in the Tengger Desert, under the condition of the constant average principal stress, p, were conducted by an equivalent alternative method to achieve a true triaxial stress path by a pseudo-triaxial apparatus. The results show that the method can better determine the strength. The peak shear stress decreases gradually with the increase of the intermediate principal stress coefficient, b, at the same p. Compared with the SMP and Mohr–Coulomb criteria, the peak shear stress is near the strength lines predicted by both criteria. At a lower p, the specimen exhibited strain-softening behaviours, but at a higher p, it showed hardening behaviours. Under the conditions of a higher p and lower b, the specimen exhibited contraction first and then dilatancy. The specimen deformation is greatly affected by anisotropy, and as the p-value increases, the effect of the initial anisotropy on the specimen begins to weaken. The ε_s (generalized shear strain)/η (stress ratio)-ε_s curves, can be expressed by a linear equation, of which the slope is affected by the b-value. The experiment verifies the feasibility and rationality of the equivalent method. The test data provide support for the maintenance of desert roadbeds and the sustainable development of the economy and society in ecologically fragile areas.

Keywords: aeolian sand; stress path; deviatoric plane; shear strength; deformation behaviour

Citation: Ma, Z.; Li, X. Aeolian Sand Test with True Triaxial Stress Path Achieved by Pseudo-Triaxial Apparatus. *Sustainability* **2023**, *15*, 8328. https://doi.org/10.3390/su15108328

Academic Editors: Yutao Pan, Qiujing Pan and Hui Xu

Received: 20 April 2023
Revised: 11 May 2023
Accepted: 17 May 2023
Published: 19 May 2023

1. Introduction

About 36 million square kilometres, or 24 percent of the Earth's total land area, is desertified globally. With human activities, many projects are constructed in the desert, such as the construction of the desert highway. However, the special properties of aeolian sand make it easy for subgrades to produce sustainable settlements, which leads to embankment and foundation construction failures, which then seriously affects the sustainability of highway operations. Aeolian sand is a special roadbed filler that is widely distributed in desert areas; however, there are only a few basic experiments. In particular, its three-dimensional mechanical characteristics have received little attention. For studying the three-dimensional mechanical behavior of soil, the true triaxial apparatus (TTA) is a popular device that controls three orthogonal directions for loading independently and provides a software and hardware basis for determining the soil's mechanical behaviour in three dimensions. The pseudo-triaxial specimen (PTA) is loaded in an axisymmetric stress state, which can only control the stress in the axial and radial directions independently. Therefore, the PTA cannot measure the influence of the intermediate principal stress on the deformation and strength, which severely limits its measurement. However, the development of the TTA overcomes the crucial defect of the PTA, theoretically, and becomes an ideal device for element testing.

Since Kjellman [1] first designed a TTA, it has opened a new era in the study of the three-dimensional mechanical behaviours of soil, as shown by Bishop [2], who tested it on

dry sand, Ko et al. [3] and Alshibli et al. [4], who tested it on Ottawa sand, Lade et al. [5], who tested it on Monterey sand, Gao et al. [6], who tested it on Toyoura sand, Zhang et al. [7], who tested it on standard sand, and Li et al. [8,9], who tested it on aeolian sand at different confining pressures and different intermediate principal stress coefficients. These test results show that the peak of the internal friction angle first increases and then decreases with the increase of b. The peak internal friction angle of triaxial tension is significantly higher than that of triaxial compression. Moreover, sand dilatation is also significantly affected by the intermediate principal stress and the anisotropy characteristics. The results obtained by Nakai et al. [10], Reddy et al. [11], Matsuoka et al. [12], and Choi et al. [13] for different soils with a constant p show that soil deformations are directly bound up with the stress path. In addition, Shao et al. [14] studied the lateral deformation characteristics of soil in the shearing process at different stress states. Suits et al. [15] and Lade et al. [16–19] conducted a true triaxial test on dense sand to study the deformation and failure characteristics of transverse isotropic sand. Lu et al. [20] simulated the true triaxial tests of Ochiai and Lade [21] on Cambria sand to study the influences of its inherent cross-anisotropy and bifurcation characteristics. Furthermore, the TTA is also adopted to carry out plane strain tests [22,23]. Some apply it to study the small strain behaviour of granular soil [24]. The TTA has been widely used in complex stress path tests to obtain soil mechanics; the constitutive theory based on the test results has also been developed by leaps and bounds. The application of the TTA has solved many complicated challenges, but unfortunately, it has not been widely popular because of its inherent problems, such as the collision of rigid loading [25], boundary friction [26,27], and measurement accuracy [28,29]. To avoid those problems, the deformation gaps are reserved [30], which will lead to uneven stress and strain [31]. The above all affect the accurate determination of soil behaviour. In contrast, the pseudo-triaxial test, which originated earlier, is simple to conduct, and most of the existing engineering applications and model validations are still based on pseudo-triaxial test data [32–35]. Based on the above analysis, Li and Ma [36] proposed a method to equivalently achieve the true triaxial stress path with the PTA, which makes it possible to study soil's mechanical behaviour in three-dimensional spaces.

Based on the proposed method, the pseudo-triaxial stress path and the true triaxial stress path are maintained to be consistent in a p-q space, and the true triaxial stress path can be equivalently achieved by the PTA. For a detailed description of the method, please refer to our patent [36]. According to this method, the PTA was used to conduct the stress path tests on aeolian sand in the Tengger Desert under drained conditions, with a p of 100 kPa, 300 kPa, 600 kPa, and 900 kPa, respectively. The purpose was to achieve the stress path at different stress states while meanwhile verifying the feasibility and rationality of the method. Furthermore, we will discuss the mechanical parameters on the deviatoric plane and the deformation characteristics of aeolian sand. The description of these features is conducive to improving the sustainability of buildings such as roadbeds.

2. Experimental Procedures

2.1. Pseudo-Triaxial Apparatus

The apparatus can carry out constant stress and constant strain control, which can achieve various static tests of soil mechanics. The schematic diagram is shown in Figure 1. Each part of the apparatus is controlled by a single-chip microcomputer, which can cooperate with computer work independently. The data acquisition apparatus can exchange data with the computer and collect and process data in real time. The constant strain control rate range is 0.002~4 mm/min, and the accuracy is ±1%. The measuring range of the axial pressure sensor is 0~30 kN, and the accuracy is ±1%. The measuring range of the confining pressure controller is 0~1.99 MPa, the measuring range of the back-pressure controller is 0~0.99 MPa, and the accuracy is ±0.5% FS (Full Scale).

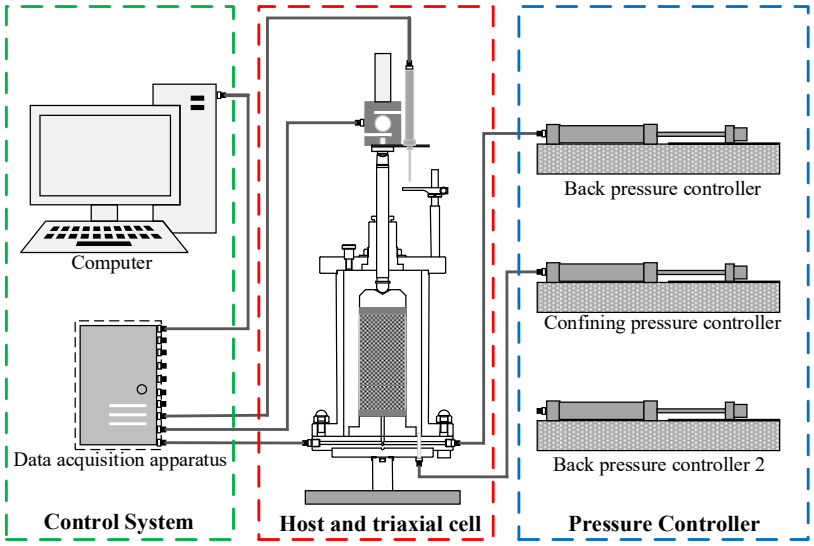

Figure 1. Schematic diagram of triaxial apparatus.

2.2. Material Parameters of Aeolian Sand

The aeolian sand was sampled from the hinterland of the Tengger Desert, China, which is widely representative. The natural moisture content was 0.14%, the maximum density was 1.68 g/cm^3, the minimum density was 1.40 g/cm^3, and the specific gravity was 2.67. Figure 2 shows the particle size distribution curve measured by a laser particle size analyser. The integral distribution (red curve) is the cumulative particle size distribution curve, and the differential distribution (blue curve) is the percentage of a particle size's mass in the total mass. From Figure 2, it can be concluded that the coarse end particle size, d_{97}, is 0.5, the constrained grain size, d_{60}, is 0.35, the median diameter, d_{30}, is 0.30, the effective grain diameter, d_{10}, is 0.26, the fine end grain size, d_3, is 0.23, the specific surface area, S/V, is 2.1 cm^2/cm^3, and the coefficient of nonuniformity, C_u, is 1.42. The coefficient of the curvature, C_c is 0.97, the fine grain content is less than 5%, and the classified aeolian sand is poorly graded sand. The particle mass with grain size larger than 0.075 mm exceeds 85% of the total mass, and the aeolian sand is classified as fine sand.

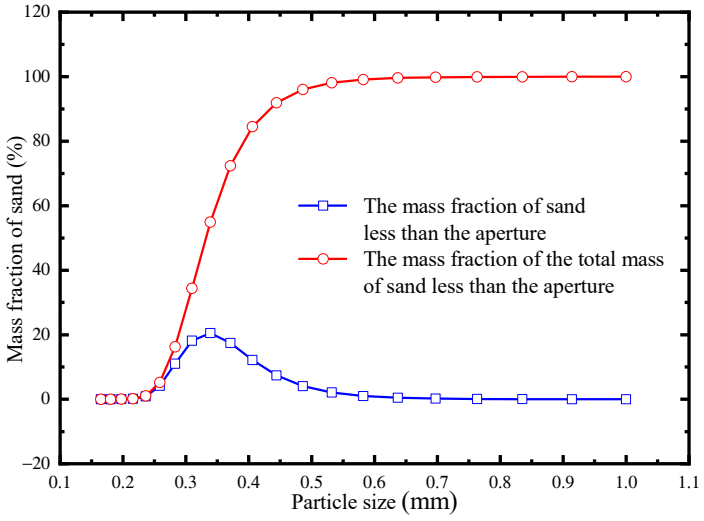

Figure 2. Particle size distribution curve of aeolian sand.

2.3. Specimen Preparation

The specimen's size was a diameter, Φ, of 39.1 mm × height 80 mm. In the process of specimen preparation, the relative density was controlled to be D_r = 0.37, the initial

void ratio was e_0 = 0.79, and the medium-density specimen with a density of 1.49 g/cm^3 was prepared. To reduce the influence of the rubber membrane, a vacuum pump was adopted to pump the air in the confined space (the space between the split mould and the rubber membrane) to make the rubber membrane close to the inner wall of the split mould. The specimens were prepared by the layered falling sand method (Figure 3). The aeolian sand was evenly dropped into the specified height so that the density of each layer of the specimen was consistent. Moreover, to reduce the error of manual specimen preparation and ensure its stability, it was necessary to control the height error of the specimen to be less than 1 mm, i.e., less than 1.5% of the specimen's height. After the specimen was prepared, the vacuum pump was transferred to the back-pressure valve, and the other valves connected to the specimen were closed. A negative pressure of 20 kPa was maintained by the vacuum pump to fix the specimen's shape. Finally, by opening the split mould, installing the triaxial cell, filling it with water, and pre-applying the confining pressure of 20 kPa, the specimen installation was completed. It should be noted that the specimen's size should be strictly controlled in the specimen preparation process. The specimen preparation method should be consistent to ensure stability and repeatability and reduce the error of manual specimen preparation.

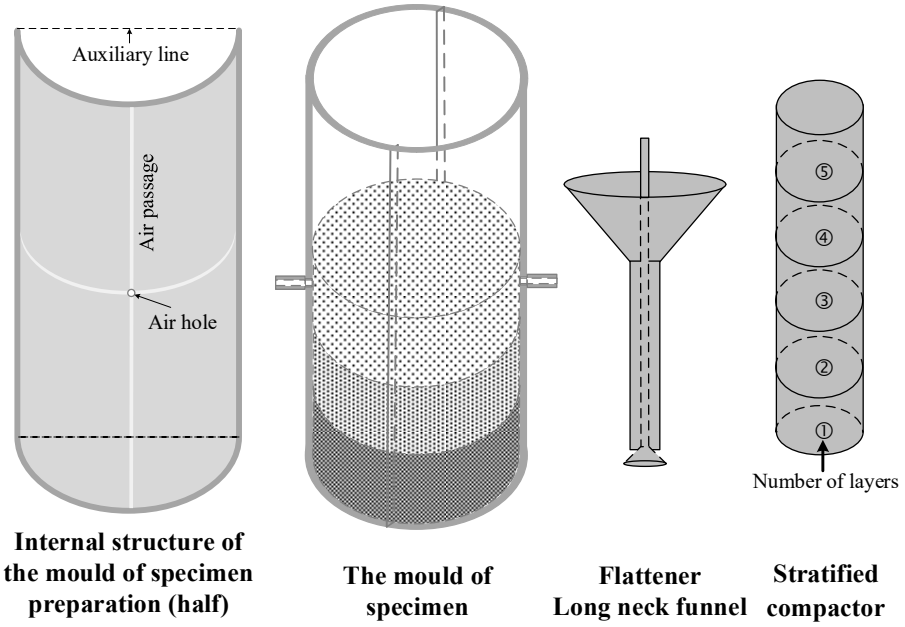

Figure 3. Specimen preparation process.

After the specimen was installed, hydrostatic head saturation and back-pressure saturation were carried out. Because the air in the specimen was compressible, it increased the difficulty of parametric measurement and reduced the reliability of the results. Therefore, the hydrostatic head saturation was carried out first, and the air in the specimen was displaced by de-aired water so that the three-phase body composed of solid, liquid, and gas became a two-phase body composed of solid and liquid. After that, back-pressure saturation was performed to eliminate the influence. When the saturability reached more than 98%, the specimen was saturated. After the saturation procedure, the specimen was subjected to isotropic consolidation, and the consolidation was considered complete when the volume of water discharged from the specimen was less than 1% within 30 min.

3. Test Method and Strength Criterion

3.1. Test Method Introduction

Testing and describing the mechanical behaviour of soil in three-dimensional space is the focus of geotechnical scholars. The TTA is an ideal device for element testing. However, it has not been widely popular because of its inherent problems. Thus, the author proposed

an equivalent alternative method to measure the three-dimensional mechanical behaviour of soil. The method can determine the spatial mechanical behaviour by a pseudo-triaxial apparatus, which significantly reduces the testing cost. An introduction to the method is as follows.

The TTA can achieve any stress path on the deviatoric plane by controlling the average principal stress, p, the generalized shear stress, q, and the Lode angle, θ_σ. Although the PTA cannot achieve the stress path directly, the stress path in the generalized stress space (the p-q space) can be kept consistent by two apparatuses simultaneously. Therefore, the PTA can equivalently achieve the same stress path as the TTA. The method proposed by the author et al. [36] adopts a PTA to keep the stress path consistent with the true triaxial stress path in the p-q space to achieve the stress path test at a different p and b, which is an equivalent alternative method, not a true triaxial test in the real sense.

The average principal stress increment, dp, and generalized shear stress increments, dq and b, at true triaxial conditions are as follows.

$$\begin{cases} \mathrm{d}p = \frac{\mathrm{d}\sigma_1+\mathrm{d}\sigma_2+\mathrm{d}\sigma_3}{3} \\ \mathrm{d}q = \frac{(2\sigma_1-\sigma_2-\sigma_3)\mathrm{d}\sigma_1-(\sigma_1-2\sigma_2+\sigma_3)\mathrm{d}\sigma_2-(\sigma_1+\sigma_2-2\sigma_3)\mathrm{d}\sigma_3}{\sqrt{2}\sqrt{(\sigma_1-\sigma_2)^2+(\sigma_2-\sigma_3)^2+(\sigma_1-\sigma_3)^2}} \\ \mathrm{d}\sigma_2 = b\mathrm{d}\sigma_1 + (1-b)\mathrm{d}\sigma_3 \end{cases} \tag{1}$$

where σ_1 is the major principal stress; σ_2 is the intermediate principal stress; σ_3 is the minor principal stress; dσ_1 is the major principal stress increment; dσ_2 is the intermediate principal stress increment; dσ_3 is the minor principal stress increment.

Here, we represent σ_2 in terms of σ_1 and σ_3 to the equivalent of the influence of σ_2. Therefore, Equation (2) is obtained from Equation (1) and reads:

$$\mathrm{d}p = \frac{(1+b)\mathrm{d}\sigma_1 + (2-b)\mathrm{d}\sigma_3}{3} \tag{2}$$

According to Equation (2), if it is required to achieve a constant p loading at a different b, that is, dp = 0, then:

$$\mathrm{d}\sigma_3 = \frac{b+1}{b-2}\mathrm{d}\sigma_1 \tag{3}$$

If b is regarded as a proportional coefficient, and σ_1 and σ_3 are controlled using the PTA, it can be drawn from Equation (3) that the stress paths consistent with true triaxial stress paths can be achieved equivalently by controlling σ_1 increases and σ_3 decreases proportionally.

3.2. Strength Criterion

To reveal the peak strength of aeolian sand on the deviatoric plane and verify the feasibility and rationality of the method, two widely popular Mohr–Coulomb criteria were adopted to compare and analyse the peak points in this paper.

The general expression for the Mohr–Coulomb is as follows.

$$q - M_f g(\theta_\sigma) p = 0 \tag{4}$$

where M_f is the peak stress ratio of the triaxial test (b = 0, $\theta_\sigma = -30°$); $g(\theta_\sigma)$ is the shape function. The expressions for M_f are as follows.

$$\begin{cases} M_f = \frac{6\sin\varphi_f}{3-\sin\varphi_f} (b = 0,\ \theta_\sigma = -30°) \\ M_f = \frac{6\sin\varphi_f}{3+\sin\varphi_f} (b = 1,\ \theta_\sigma = 30°) \end{cases} \tag{5}$$

where φ_f is the peak internal friction angle.

The first is the spatially mobilized plane (SMP) obtained by Matsuoka and Nakai [37], and its shape function, $g(\theta_\sigma)$, is as follows.

$$g(\theta_\sigma) = \frac{\sqrt{3}}{2} \frac{\beta}{\sqrt{\beta^2 - \beta + 1}} \frac{1}{\cos\alpha} \tag{6}$$

where

$$\alpha = \begin{cases} \frac{1}{6}\cos^{-1}(-1 + \frac{27}{2}\frac{\beta^2(1-\beta)^2}{(\beta^2-\beta+1)^3}\sin^2 3\theta_\sigma) & , \theta_\sigma \le 0 \\ \frac{\pi}{3} - \frac{1}{6}\cos^{-1}(-1 + \frac{27}{2}\frac{\beta^2(1-\beta)^2}{(\beta^2-\beta+1)^3}\sin^2 3\theta_\sigma) & , \theta_\sigma > 0 \end{cases}$$

where β is the ratio of the peak stress while θ_σ is 30° and −30°, respectively, and reads.

$$\beta = \frac{\left(M_f\right)_{\theta_\sigma=30^\circ}}{\left(M_f\right)_{\theta_\sigma=-30^\circ}} \tag{7}$$

The second is the Mohr–Coulomb criterion obtained by Bardet [38] using a linear interpolation function, and its expression is as follows.

$$g(\theta_\sigma) = \frac{\sqrt{3}\beta}{(\beta+1)\cos\theta_\sigma + \sqrt{3}(\beta-1)\sin\theta_\sigma} \tag{8}$$

4. Test Scheme and Results

4.1. Stress Path Test Scheme

To study the strength and deformation characteristics of aeolian sand on the deviatoric plane, a PTA was adopted to conduct a stress path test at the drained condition when p was 100, 300, 600, and 900 kPa, and b was 0, 0.2, 0.4, 0.6, 0.8, and 1, respectively. The test scheme is shown in Table 1.

Table 1. Test scheme at constants p and b.

***p*(kPa)**	***b***	**Loading Method**
100 300 600 900	0 0.2 0.4 0.6 0.8 1	The test adopts stress-controlled loading, and the constant p loading is achieved by controlling the increase of σ_1 and the decrease of σ_3; by controlling the increase rate of σ_1 and the decrease rate of σ_3, loading schemes of different b are achieved, i.e., $\Delta\sigma_3 = (b + 1)/(b - 2)\cdot\Delta\sigma_1$; the control ratios of σ_1 and σ_3 are shown in Figure 4.

In the test, it is necessary to control the increasing rate of σ_1 and the decrease rate of σ_3 to load according to the set ratio (Equation (3)) so that the stress path's loading scheme of different b at the condition of a constant p can be achieved. Figure 5 is a schematic diagram of the stress path after being processed by the proposed method in the deviatoric plane. Figure 6 is a schematic diagram of the actual stress path's loading by PTA in the p-q space.

There are many influencing factors in the actual test process. To accurately verify the method and reveal the strength and deformation of aeolian sand, it is necessary to keep all of the controllable influence parameters completely consistent, such as the specimen preparation method and the specimen's compactness, saturation, consolidation conditions, loading rate, etc. The influence of the uncontrollable influence parameters should be minimized as much as possible.

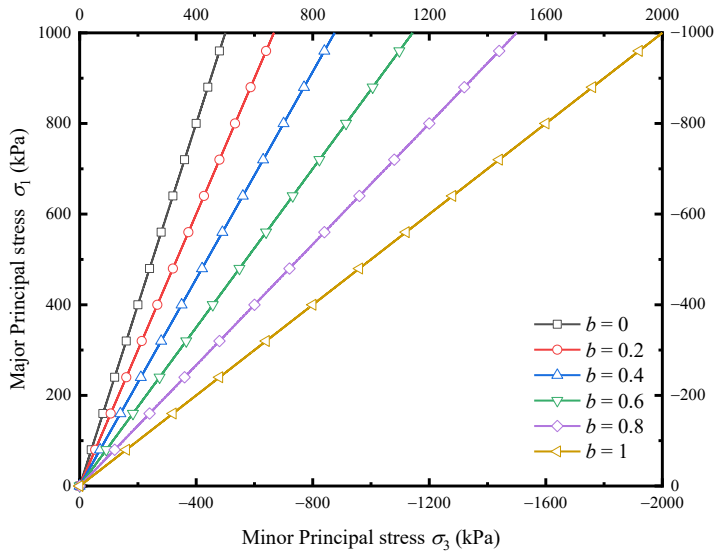

Figure 4. Schematic diagram of stress loading path.

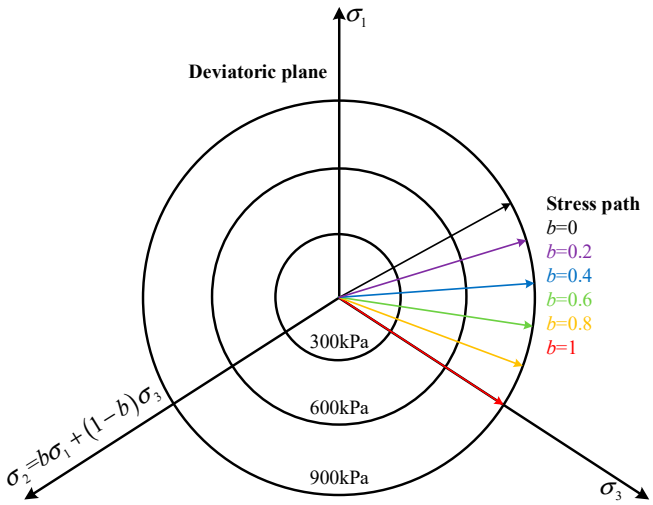

Figure 5. The stress path after being processed.

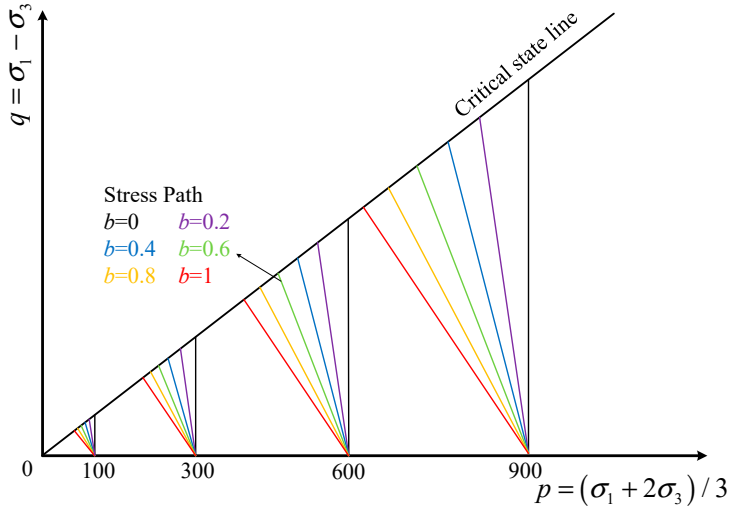

Figure 6. The designed stress path's loading by pseudo-triaxial.

4.2. Stress Path Test Results

Figure 7 shows the effective stress paths measured by a PTA at different loading conditions. Figure 8 shows the stress path with a constant p, processed by the proposed method in the same test conditions. The information in Figure 7 shows that the peak stress ratio of aeolian sand varies from 1.44 to 1.47 as b increases, with a change rate of about 2% and an average peak stress ratio of about 1.46, which is almost consistent. The results show that aeolian sand has a unified critical state.

At the same p, the slope of the measured stress path gradually increases as b increases, but the slope of the critical state line gradually decreases (Figure 7). The peak stress ratio is significantly affected by the b-value, i.e., as the b-value increases, the peak stress ratio decreases. Figure 8 shows that all the stress paths of different b processed by the proposed method always remain plumb lines perpendicular to the p-axis. The stress path is always loaded along the design path, which shows that the method is feasible and controllable. Based on the above analysis, it is concluded that the equivalent stress paths can be achieved accurately by a PTA. When comparing the slope of the critical state line, the difference is more than 10%.

Figure 9a–d show the variation of q with an axial strain, ε_1, and a radial strain, ε_3, at p = 100, 300, 600, and 900 kPa. In all the q~ε_1 curves, q gradually decreases after reaching the peak value, and the q~ε_1 curves show a strain-softening, indicating that p has a great influence on the curve shapes. As p increases, the peak strength at the same b increases gradually, and the strain corresponding to the peak strength increases. For example, when p = 100 kPa, b = 0, the shear stress peaks at a strain of about 2.5%, while when p = 300, 600, and 900 kPa, b = 0, and the shear stress peaks at a strain of about 7%, 10%, and 12%, respectively. Moreover, the q~ε_1 curves at other b also have similar laws. At the same p (such as p = 600 kPa, Figure 9c), the peak of q gradually decreases as b increases, and the corresponding ε_1 gradually decreases while the peak is reached. The curves at other p (p = 100, 300, and 900 kPa) also have similar variation laws. This is consistent with the mechanical properties and with the peak strength measured by true triaxial tests.

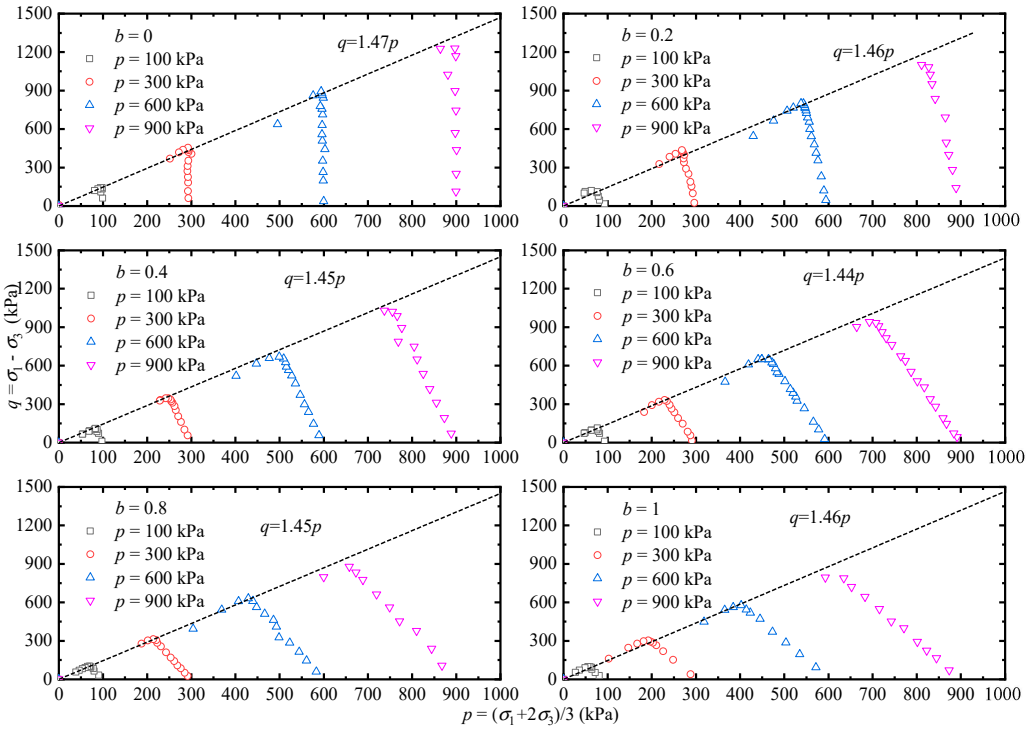

Figure 7. Effective stress path measured by pseudo-triaxial apparatus.

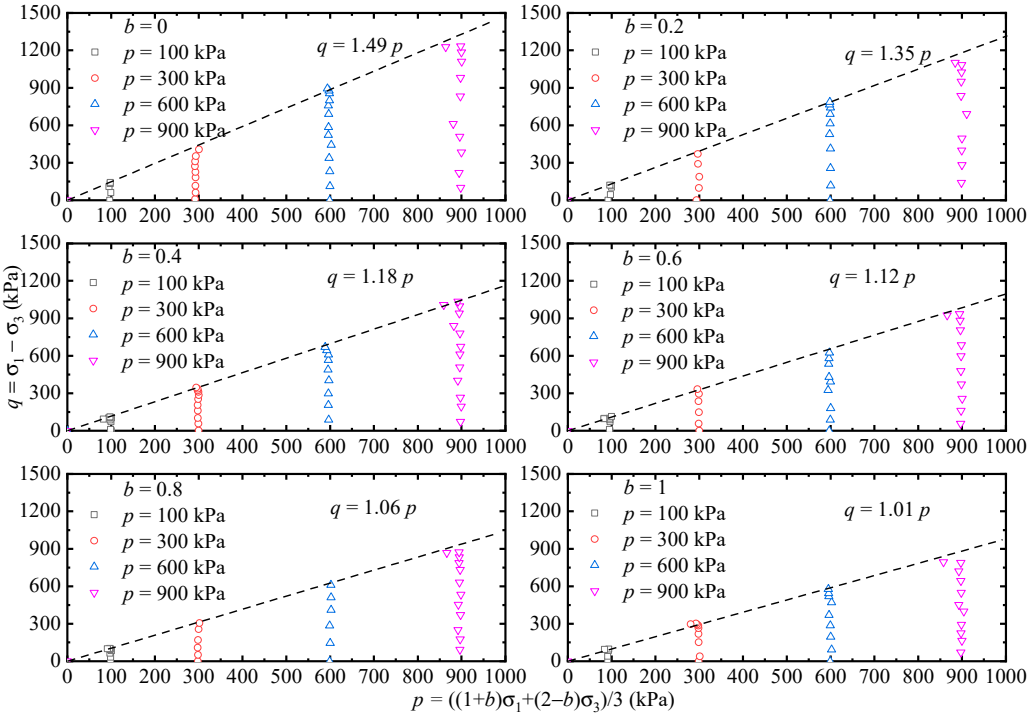

Figure 8. Effective stress path processed by the proposed method.

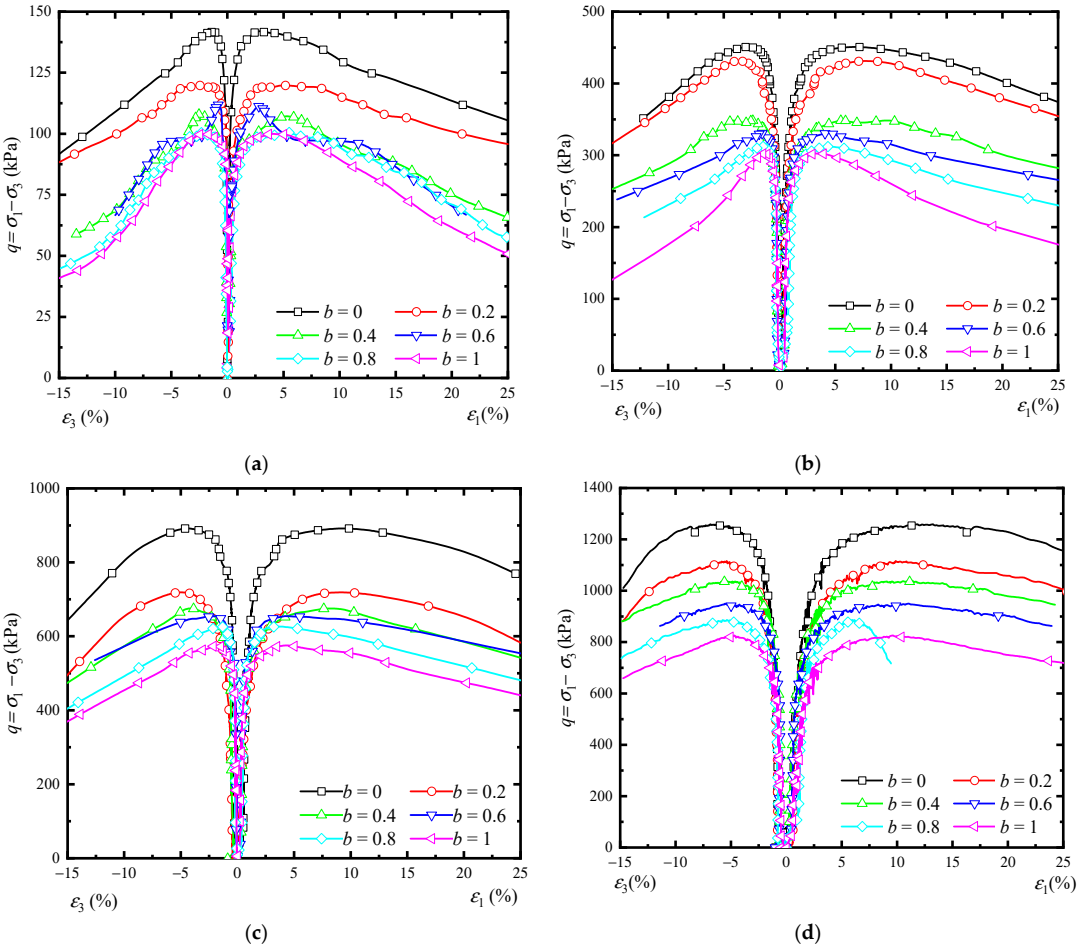

Figure 9. Relationships between principal strain component and deviatoric stress at the same p and different b. (**a**) p = 100 kPa. (**b**) p = 300 kPa. (**c**) p = 600 kPa. (**d**) p = 900 kPa.

Figure 10a–d show the variation of volumetric strain, ε_v and ε_1, at p = 100, 300, 600, and 900 kPa. It can be concluded that ε_v is greater than 0 at p = 100 kPa and 300 kPa, and the specimen only occurs at dilatation. The ε_v-ε_1 curves at different b have a crossover phenomenon (Figure 10a,b). Only at p = 600 kPa and p = 900 kPa does the ε_v decrease first, and then it increases with the ε_1 at different b, i.e., the specimen contracts first and then dilates. The contraction is most remarkable at b = 0 and 0.2 and weaker at other b, indicating that the deformation and failure modes are greatly influenced by the test conditions of the constants p and b (Figure 10c,d). In conclusion, the deformation failure mode of aeolian sand is mainly dilatancy, and it also shows the contraction first and then dilatancy when p is larger and b is smaller.

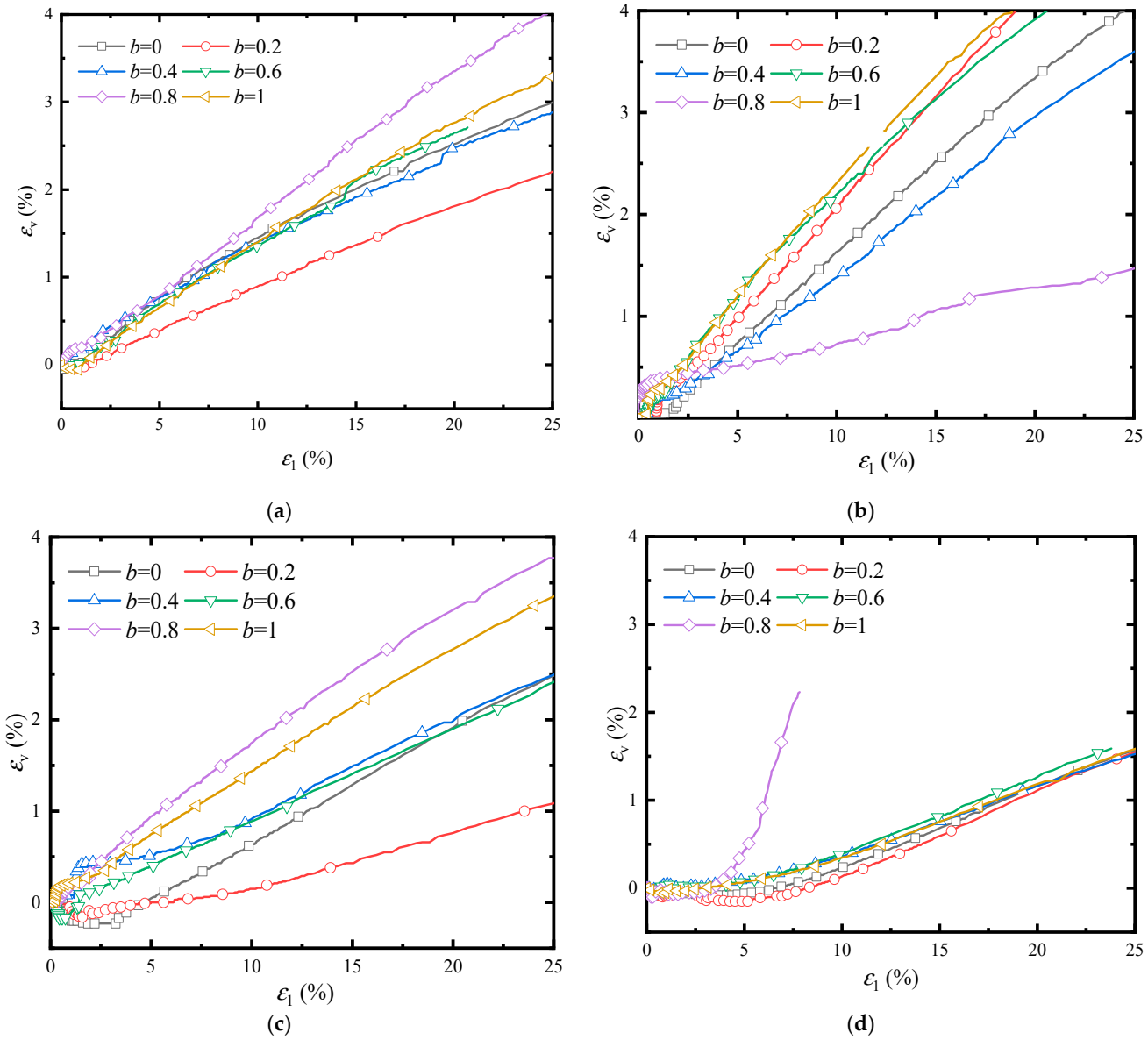

Figure 10. Relationships between ε_v and ε_1 at the same p and different b. (**a**) p = 100 kPa. (**b**) p = 300 kPa. (**c**) p = 600 kPa. (**d**) p = 900 kPa.

Figure 11a–d show the relationships between ε_3 and ε_1 at different loading conditions. The ε_1-ε_3 curves show a linear variation, and their slopes are different, indicating that the deformation degree of the axial and radial is significantly affected by p and b. In addition, there is no obvious proportional relationship between the values of ε_3 and ε_1 at the same b, which is caused by the initial anisotropy of aeolian sand during specimen preparation.

However, at p = 900 kPa, the slopes of the ε_1-ε_3 curves are almost the same, and the value of ε_1 and ε_3 satisfies the proportional relationship of $\varepsilon_1 \approx -2\varepsilon_3$, which indicates that the deformation of the specimen deforms uniformly at this condition and is almost in an isotropic state.

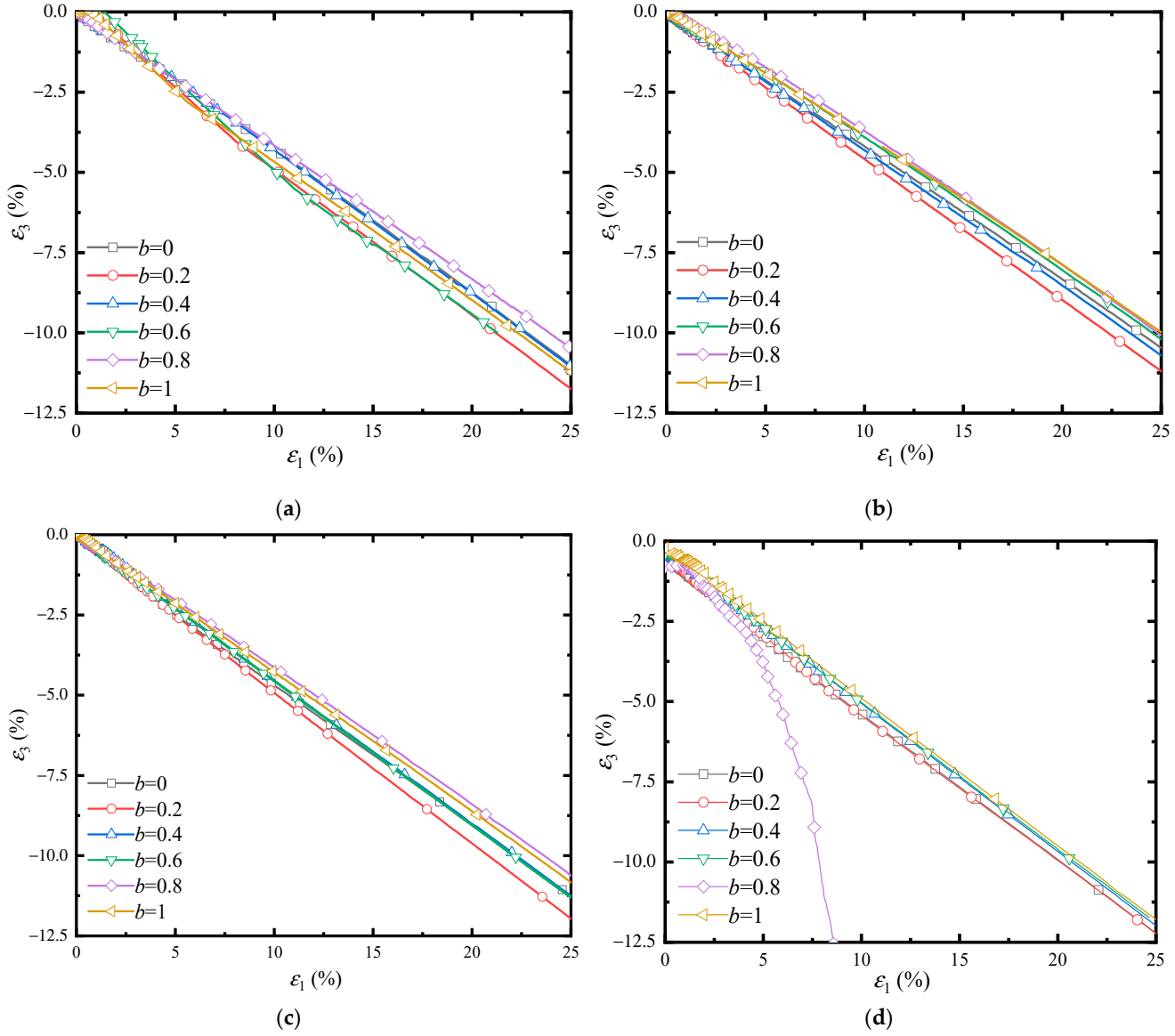

Figure 11. Relationships between ε_3 and ε_1 at the same p and different b. (**a**) p = 100 kPa. (**b**) p = 300 kPa. (**c**) p = 600 kPa. (**d**) p = 900 kPa.

Figure 12a–d show the generalized stress ratio, η~, and generalized shear strain, ε_s, relationships and the ε_s/η~ε_s relationships at p = 100, 300, 600, and 900 kPa. The expressions for η and ε_s are as follows.

$$\eta = \frac{q}{p} \tag{9}$$

$$\varepsilon_s = \frac{\sqrt{2}}{3}\sqrt{(\varepsilon_1 - \varepsilon_2)^2 + (\varepsilon_2 - \varepsilon_3)^2 + (\varepsilon_3 - \varepsilon_1)^2} \tag{10}$$

where $\varepsilon_2 = \varepsilon_3$. Compared with Figure 12(a1–d1), it can be concluded that the peak value of η decreases with the increase of b, which is consistent with the variation law of the true triaxial test in the same loading conditions.

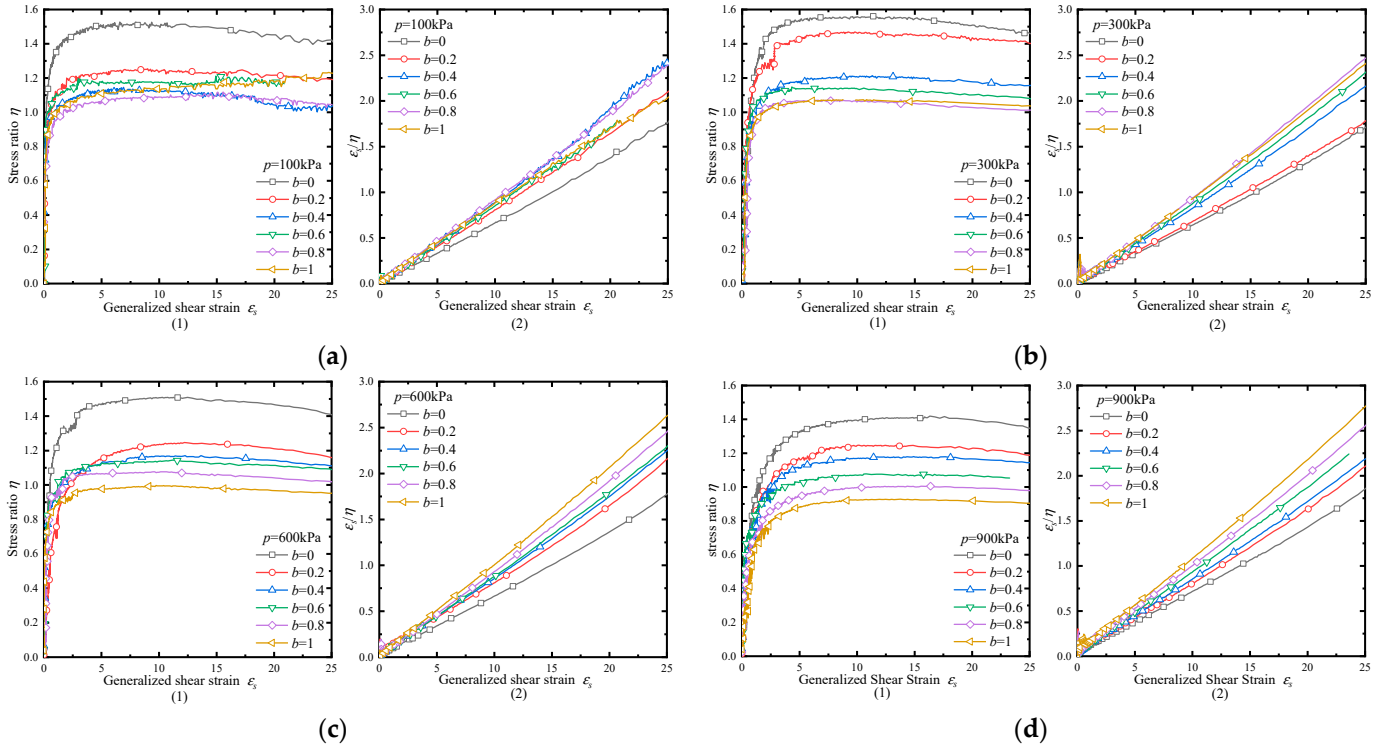

Figure 12. Relationships between stress ratio and ε_s/η with generalized shear strain ε_s. (**a**) p = 100 kPa. (**b**) p = 300 kPa. (**c**) p = 600 kPa. (**d**) p = 900 kPa.

At the same b and different p, the peak values of η are almost consistent, indicating that the aeolian sand has a unified critical state. Comparing Figure 12(a2–d2), it can be concluded that the curve of ε_s/η~ε_s changes linearly, which can be expressed by the straight-line equation proposed by Sun et al. [39] as follows.

$$\frac{\varepsilon_s}{\eta} = m + n\varepsilon_s \tag{11}$$

where m is the intercept of the straight-line equation on the ε_s/η-axis; n is the slope of the straight-line equation. The test results in this paper are consistent with the description of the equation proposed by Sun et al. [39]. In fact, Equation (11) adopts the generalized stress ratio, η, to express the strain-softening characteristics of the test curve. It can be drawn from Figure 12 that m is almost unchanged at all conditions, i.e., the value of m has nothing to do with b. However, the change of n is more remarkably affected by b and p, i.e., n increases with the increase of b at the same p, and n also increases with the increase of p, indicating that the strain-softening phenomenon is enhanced, and the stress–strain relationships are affected by both p and b.

Figure 13a–d show the test peak shear stress of aeolian sand at different loading conditions and the predicted strength lines on the deviatoric plane of two modified Mohr–Coulomb strength criteria determined according to the test parameters when b = 0 and b = 1. By comparing the strength lines predicted by the two strength criteria with the strong trajectory of the test peak shear stress point on the deviatoric plane (Figure 13), it can be drawn that the SMP criterion can better predict the changing trend, while Bardet's Mohr–Coulomb criterion has a more conservative prediction line, i.e., the predicted value is lower than the test peak stress point. The test results better reveal the strength of the deviatoric plane, which again proves the feasibility and rationality of the method, i.e., that pseudo-triaxial tests can equivalently achieve the same stress path as the true triaxial test in a generalized stress space.

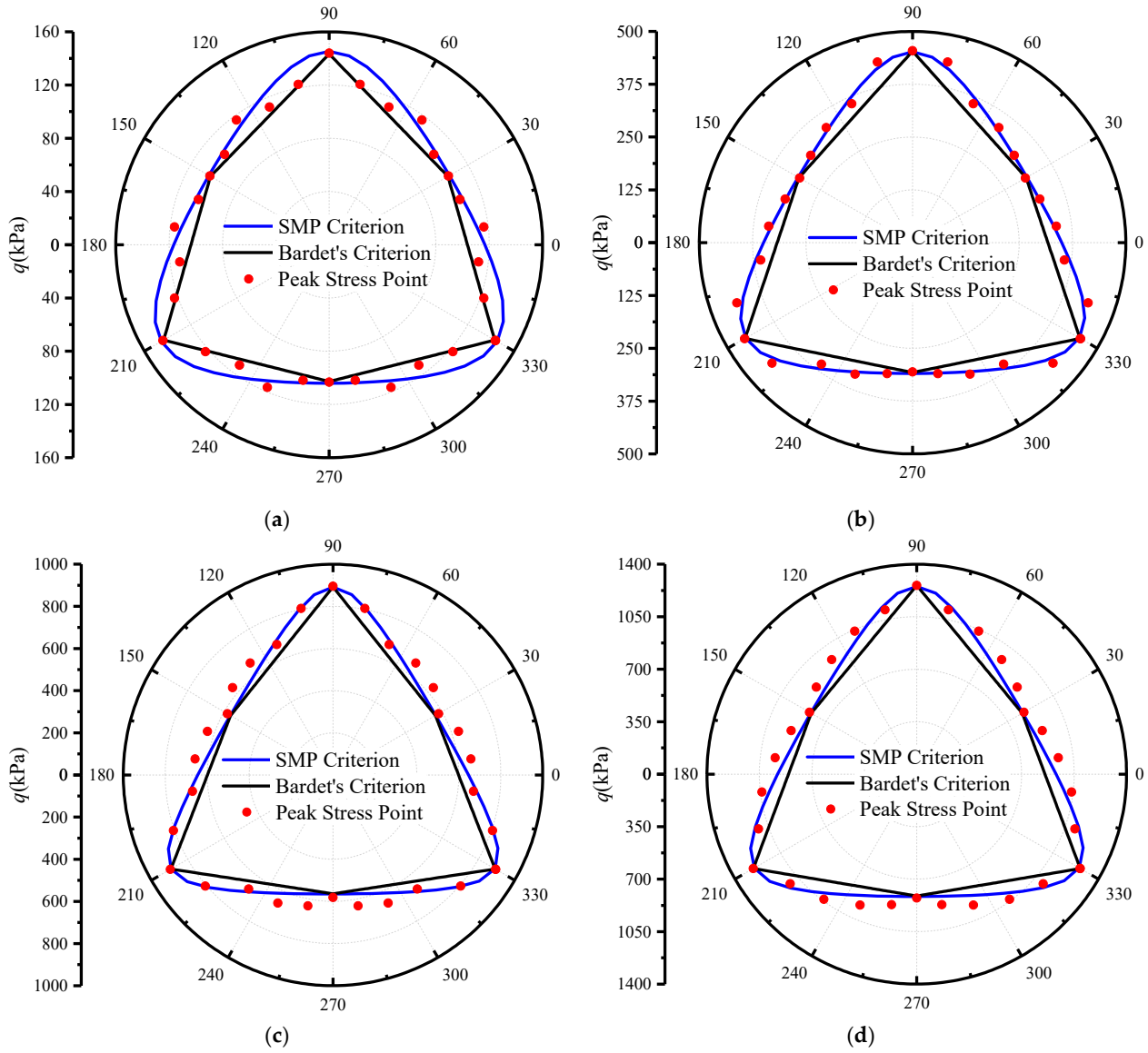

Figure 13. Comparison of peak strength of aeolian sand with Mohr–Coulomb criterion. (**a**) p = 100 kPa. (**b**) p = 300 kPa. (**c**) p = 600 kPa. (**d**) p = 900 kPa.

5. Conclusions and Discussion

Based on one of the methods proposed by the author, the true triaxial stress path in a generalized stress space was equivalently achieved by pseudo-triaxial tests, and the strength on the deviatoric plane and deformation of aeolian sand were measured. The measurement of these parameters is of great benefit to the sustainability of roadbeds and other buildings in desert areas. The main conclusions are as follows.

(1) The strength on the deviatoric plane in the equivalent study of the pseudo-triaxial test is similar to the characteristics measured by the true triaxial test, i.e., the peak shear stress decreases as b increases. It is shown that the PTA can equivalently achieve some stress paths of the TTA. The test results have verified the feasibility and rationality of the proposed method, indicating that the PTA can equivalently achieve some functions of the TTA.

(2) The deformation failure mode of aeolian sand is mainly dilatancy at the lower p, and it also shows the contraction first and then dilatancy when p is larger and b is smaller. The deformation and failure modes are affected by p, q, and b, and the influence of the three factors needs to be considered comprehensively.

(3) At the lower p, the linear relationship between ε_3 and ε_1 changes with b, and the deformation degree in different directions are different, which is significantly affected by the initial anisotropy. The ε_s/η-ε_s relationships can be described by a unified linear equation. At the same p, the slope of the ε_s/η-ε_s curve increases with the increase of b, and the strain-softening phenomenon is enhanced. The stress–strain relationships are affected by both p and b.

(4) Compared with the predicted strength lines of the SMP and Mohr–Coulomb criterion, the peak shear stress points are evenly distributed near the predicted failure surface, which better represents the peak strength characteristics at the special stress paths. The test results, once again, demonstrate the feasibility and rationality of achieving a three-dimensional stress path on the deviatoric plane with the PTA.

6. Patents

According to the method proposed by the author et al. in our patent, a series of validation tests were carried out for this paper. For details of the method, please refer to our patent "A method to achieve the three-dimensional space stress or strain path by pseudo-triaxial apparatus", No: CN202111429048.0; Authorized.

Author Contributions: Conceptualization: X.L. and Z.M.; Methodology: X.L. and Z.M.; Formal analysis and investigation: X.L. and Z.M.; Writing—original draft preparation: Z.M.; Writing—review and editing: Z.M. and X.L.; Funding acquisition: X.L.; Resources: X.L.; Supervision: X.L. All authors have read and agreed to the published version of the manuscript.

Funding: This work was financially supported by the Projects for Leading Talents of Science and Technology Innovation of Ningxia (No. KJT2019001), the National Natural Science Foundation of China (No. 121602028), the innovation team for multi-scale mechanics and its engineering applications of the Ningxia Hui Autonomous Region (2021), and these supports are gratefully acknowledged.

Institutional Review Board Statement: Not applicable.

Informed Consent Statement: Informed consent was obtained from all subjects involved in the study.

Data Availability Statement: The data used to support the findings of this study are available from the corresponding author upon request.

Conflicts of Interest: The authors declare no conflict of interest.

References

1. Kjellman, W. Report on an apparatus for consummate investigation of the mechanical properties of soils. In Proceedings of the 1st International Conference on Soil Mechanics and Foundation Engineering, Cambridge, MA, USA, 22–26 June 1936; Volume 2, pp. 16–20.
2. Bishop, A.W. The strength of soils as engineering materials. *Geotechnique* **1966**, *16*, 91–130. [CrossRef]
3. Ko, H.Y.; Scott, R.F. Deformation of sand at failure. *J. Soil Mech. Found. Div.* **1968**, *94*, 883–898. [CrossRef]
4. Alshibli, K.A.; Williams, H.S. A true triaxial apparatus for soil testing with mixed boundary conditions. *Geotech. Test. J.* **2005**, *28*, 534–543.
5. Lade, P.V.; Duncan, J.M. Cubical triaxial tests on cohesionless soil. *J. Soil Mech. Found. Div.* **1973**, *99*, 793–812. [CrossRef]
6. Gao, Y.; Wang, Y.H.; Su, J. Experimental characterization of the influence of fines on the stiffness of sand with inherent fabric anisotropy. *Soils Found.* **2015**, *55*, 1148–1157. [CrossRef]
7. Zhang, M.; Xu, C.S.; Du, X.L.; Wang, G.S.; Lu, D.C. True triaxial experimental research on shear behaviors of sand under different intermediate principal stresses and different stress paths. *J. Hydraul. Eng.* **2015**, *46*, 1072–1079. (In Chinese)
8. Li, X.; Ma, Z.; Lu, W.; Wang, Y. True-triaxial drained test of Tengger Desert sand. Advances in Civil Engineering. *Adv. Civ. Eng.* **2020**, *2020*, 8851165. [CrossRef]
9. Li, K.F.; Li, X.F.; Chen, Q.S.; Nimbalkar, S. Laboratory Analyses of Non-coaxiality and Anisotropy of Spherical Granular Media under True Triaxial State. *Int. J. Geomech.* **2023**.
10. Nakai, T.; Matsuoka, H.; Okuno, N.; Tsuzuki, K. True triaxial tests on normally consolidated clay and analysis of the observed shear behavior using elastoplastic constitutive models. *Soils Found.* **1986**, *26*, 67–78. [CrossRef]
11. Reddy, K.R.; Saxena, S.K.; Budiman, J.S. Development of a true triaxial testing apparatus. *Geotech. Test. J.* **1992**, *15*, 89–105.
12. Matsuoka, H.; Sun, D.A. Extension of spatially mobilized plane (SMP) to frictional and cohesive materials and its application to cemented sands. *Soils Found.* **1995**, *35*, 63–72. [CrossRef] [PubMed]

13. Choi, C.; Arduino, P.; Harney, M.D. Development of a true triaxial apparatus for sands and gravels. *Geotech. Test. J.* **2008**, *31*, 32–44.
14. Shao, S.J.; Xu, P.; Shao, S.; Chen, F. Improvement and strength testing of true tri-axial apparatus with one chamber and four cells and rigid-flexible-flexible loading boundary mechanism-True triaxial apparatus developed in Xi'an University of Technology. *Chin. J. Geotech. Eng.* **2017**, *39*, 1575–1582. (In Chinese)
15. Suits, L.D.; Sheahan, T.C.; Ibsen, L.B.; Prasstrup, U. The danish rigid boundary true triaxial apparatus for soil testing. *Geotech. Test. J.* **2002**, *25*, 254–265.
16. Lade, P.V. Failure criterion for cross-anisotropic soils. *J. Geotech. Geoenvironmental Eng.* **2008**, *134*, 117–124. [CrossRef]
17. Abelev, A.V.; Lade, P.V. Effects of cross anisotropy on three-dimensional behavior of sand. i: Stress–strain behavior and shear banding. *J. Eng. Mech.* **2003**, *129*, 160–166. [CrossRef]
18. Abelev, A.V.; Lade, P.V. Characterization of failure in cross-anisotropic soils. *J. Eng. Mech.* **2004**, *130*, 599–606. [CrossRef]
19. Rodriguez, N.M.; Lade, P.V. True triaxial tests on cross-anisotropic deposits of fine Nevada sand. *Int. J. Geomech.* **2013**, *13*, 779–793. [CrossRef]
20. Lu, X.; Huang, M.; Qian, J. The onset of strain localization in cross-anisotropic soils under true triaxial condition. *Soils Found.* **2011**, *51*, 693–700. [CrossRef]
21. Ochiai, H.; Lade, P.V. Three-dimensional behaviour of sand with anisotropic fabric. *J. Geotech. Eng. ASCE* **1983**, *109*, 1313–1328. [CrossRef]
22. Wang, H.; Li, L.; Li, J.; Sun, D. Drained expansion responses of a cylindrical cavity under biaxial in situ stresses: Numerical investigation with implementation of anisotropic S-CLAY1 model. *Can. Geotech. J.* **2022**, *60*, 198–212. [CrossRef]
23. Zhang, Y.; Shao, S.J.; Chen, F.; Ding, X.; Zhang, S.J. Experimental study of strength characteristics and failure modes of Q_3 intact loess under different stress paths. *Rock Soil Mech.* **2017**, *38*, 99–106. (In Chinese)
24. Anhdan, L.; Koseki, J. Small strain behaviour of dense granular soils by true triaxial tests. *Soils Found.* **2012**, *45*, 21–38. [CrossRef] [PubMed]
25. Suits, L.D.; Sheahan, T.C.; Yin, J.H.; Zhou, W.H.; Cheng, C.M. A rigid-flexible boundary true triaxial apparatus for testing soils in a three-dimensional stress state. *Geotech. Test. J.* **2011**, *34*, 102886. [CrossRef]
26. Shi, L.; Li, X.; Bai, B.; Li, Q.; Feng, X. Numerical analysis of loading boundary effects in Mogi-type true triaxial tests. *True Triaxial Test. Rocks* **2012**, *4*, 19–32.
27. Zhang, S.; Wu, S.; Zhang, G. Strength and deformability of a low-porosity sandstone under true triaxial compression conditions. *Int. J. Rock Mech. Min. Sci.* **2020**, *127*, 104204. [CrossRef]
28. Wang, C.; Liu, Z.; Zhou, H.; Wang, K.; Shen, W. A novel true triaxial test device with a high-temperature module for thermal-mechanical property characterization of hard rocks. *Eur. J. Environ. Civ. Eng.* **2022**, *27*, 1697–1714. [CrossRef]
29. Feng, X.T.; Zhang, X.; Kong, R.; Wang, G. A novel Mogi type true triaxial testing apparatus and its use to obtain complete stress–strain curves of hard rocks. *Rock Mech. Rock Eng.* **2016**, *49*, 1649–1662. [CrossRef]
30. Green, G.E. Strength and deformation of sand measured in an independent stress control cell. In Proceedings of the of Roscoe Memorial Symposium on Stress-Strain Behaviour of Soils, Cambridge, UK, 29–31 March 1971.
31. Green, G.E. *Strength and Compressibility of Granular Materials under Generalised Strain Condition*; University of London: London, UK, 1969.
32. Zhou, H.; Hu, Q.; Yu, X.; Zheng, G.; Liu, X.; Xu, H.; Yang, S.; Liu, J.; Tian, K. Quantitative bearing capacity assessment of strip footings adjacent to two-layered slopes considering spatial soil variability. *Acta Geotech.* **2023**, 1–15. [CrossRef]
33. Li, X.; Du, C.; Wang, X.; Zhang, J. Quantitative Determination of High-Order Crack Fabric in Rock Plane. *Rock Mech. Rock Eng.* **2023**, 1–10. [CrossRef]
34. Lade, P.V.; Duncan, J.M. Elastoplastic stress-strain theory for cohesionless soil. *J. Geotech. Eng. Div.* **1975**, *101*, 1037–1053. [CrossRef]
35. Desai, C.S.; Faruque, M.O. Constitutive model for (geological) materials. *J. Eng. Mech.* **1984**, *110*, 1391–1408. [CrossRef]
36. Li, X.; Ma, Z. Method for Achieving Stress or Strain Path in Three-Dimensional Space with Pseudo-Triaxial Apparatus. Chinese Patent CN 114235571 B, 9 May 2023. Available online: https://pss-system.cponline.cnipa.gov.cn/documents/detail?prevPageTit=changgui (accessed on 9 May 2023).
37. Matsuoka, H.; Nakai, T. Stress-deformation and Strength Characteristics of Soil Under Three Different Principal Stress. *Proc. Jpn. Soc. Civ. Eng.* **1974**, *232*, 59–70. [CrossRef] [PubMed]
38. Warnke, K.W.E.; Warnke, E.P. Constitutive model for triaxial behaviour of concrete. In Proceedings of the International Association for Bridge and Structural Engineering, Zurich, Switzerland, 18–21 January 1975; pp. 1–30.
39. Sun, Y.; Pu, J.; Li, G. Effect of different stress paths on stress-strain relationship of sand. *Chin. J. Geotech. Eng.* **1987**, *6*, 78–88. (In Chinese)